SCIENCE CHINA
Chemistry

•ARTICLES•

April 2024 Vol.67 No.4: 1224–1228
https://doi.org/10.1007/s11426-023-1872-5

Supramolecular polymer network constructed by a functionalized polyimidazolium salt derived from metal-carbene template approach

Ming-Ming Gan, Zi-En Zhang, Yi-Fan Zhang, Heng Zhang, Li-Ying Sun & Ying-Feng Han*

Key Laboratory of Synthetic and Natural Functional Molecule Chemistry of the Ministry of Education, Xi'an Key Laboratory of Functional Supramolecular Structure and Materials, College of Chemistry and Materials Science, Northwest University, Xi'an 710127, China

Received October 15, 2023; accepted November 9, 2023; published online March 5, 2024

In this study, we present a supramolecular templating approach for constructing polyimidazolium salt containing crown ether and cyclobutane moieties. This strategy involves the formation of metal-carbene templates, photochemical cycloaddition, and subsequent demetallation of metal ions. Driven by the host-guest chemistry between crown ether units and ammonium salts, we successfully fabricated a supramolecular polymer **SPN1**, which features imidazolium receptors and cyclobutane units. The obtained **SPN1** demonstrates outstanding reversible stimulus-response, antibacterial behavior and conductivity.

metal-carbene template, crown ether, polyimidazolium salt, host-guest chemistry

Citation: Gan MM, Zhang ZE, Zhang YF, Zhang H, Sun LY, Han YF. Supramolecular polymer network constructed by a functionalized polyimidazolium salt derived from metal-carbene template approach. *Sci China Chem*, 2024, 67: 1224–1228, https://doi.org/10.1007/s11426-023-1872-5

1 Introduction

Supramolecular polymer networks (SPNs) are a class of soft materials with monomers crosslinked through noncovalent interactions [1–3]. Due to their dynamic nature, SPNs exhibit some unique properties, such as self-adaptability, self-healing ability, and stimuli-responsiveness [4–7]. With the remarkable growth of interest in supramolecular polymers, these materials have shown promising potential applications in artificial skins, healthcare monitoring, and stretchable electrodes [8–11]. Furthermore, adjusting the monomers used in SPNs synthesis can create systems with various properties that can be used to assress different needs [12,13]. Nevertheless, in most cases, due to the structural complexity and hierarchy of monomers involved, the systemic and efficient modulation of noncovalent interactions and functions between SPNs and monomers has become an increasingly daunting task [14–18]. Thus, it is challenging to design well-crafted synthetic building blocks to construct SPNs, especially in function-oriented synthesis.

Among the array of supramolecular interactions, host-guest recognition has shown extensive promise and attracted significant interest in the construction of SPNs due to their high directionality, remarkable selectivity, and stimuli-responsiveness [19–21]. Inspired by this, a series of supramolecular assembled receptors, including imidazolium-based cyclophanes, crown ethers, cyclodextrins, calixarenes, and pillararenes, have been designed as hosts in a precise manner stepwise self-assembly into largescale functionalized structures [22–27]. Additionally, with the introduction of specific functional groups, the resulting supramolecular polymer can attain increased structural and functional complexity [28–33]. While significant progress has been made in supramolecular polymers, the massive application potential of supramolecular polymers based on the multifunctional system still needs to be explored [34].

*Corresponding author (email: yfhan@nwu.edu.cn)

Recently, we have introduced a metal-carbene template approach (MCTA) to efficiently synthesize polyimidazolium salts with cyclobutane moieties that cannot be obtained through normal synthetic methods [35–37]. With this in mind, we designed and synthesized the extending multi-functional polyimidazolium salts with benzo-21-crown-7 (B21C7) groups *via* the efficient synthesis strategy of MCTA. Then, the host-guest interactions of crown ether units with a specific guest were further employed, leading to an SPN (Scheme 1). The obtained SPN exhibits an excellent combination of stimulus-response, antibacterial property and conductivity.

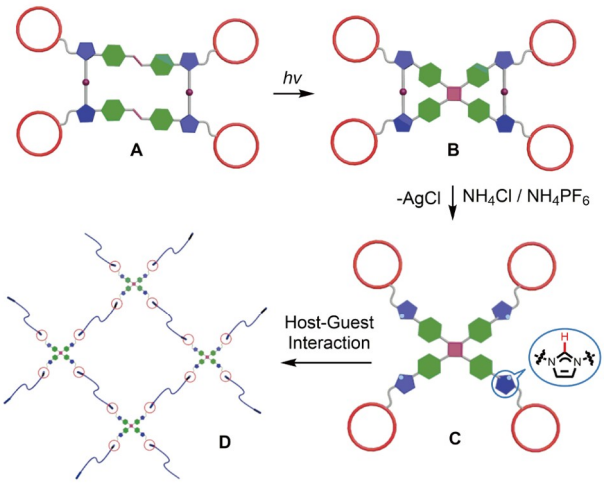

Scheme 1 Schematic representation of the formation of cross-linked SPN (**D**) from tetrakisimidazolium salt (**C**) and bisammonium salt through host-guest interaction (color online).

2 Results and discussion

2.1 Synthesis and characterization of the tetrakisimidazolium salts

Following the reported procedure, the key bisimidazolium salt H_2-**L**$(PF_6)_2$ containing B21C7 moieties was first designed and synthesized in a two-step pathway starting from (*E*)-1,2-bis(4-(1H-imidazol-1-yl)phenyl)ethene (Scheme S1, Supporting Information online) [38]. The ligand was fully characterized by ^{1}H, ^{13}C{^{1}H} nuclear magnetic resonance (NMR) spectroscopy and electrospray ionization mass spectrometry (ESI-MS) (Figures S1–S3, Supporting Information online). Typical resonance for the imidazolium C2–H proton in ^{1}H NMR spectrum was observed at δ = 9.93 ppm for H_2-**L**$(PF_6)_2$ in DMSO-d_6, and the characteristic olefin proton was shown at δ = 7.52 ppm.

The reaction of bisimidazolium salt H_2-**L**$(PF_6)_2$ with an excess of Ag_2O under the exclusion of light in acetonitrile yielded silver carbene complex $[Ag_2\mathbf{L}_2](PF_6)_2$ containing four B21C7 moieties in 89% yield (Scheme 2 and Figures S4–S9). Typically, the resonance of imidazolium C2–H proton in H_2-**L**$(PF_6)_2$ disappeared in the ^{1}H NMR spectra, indicating the formation of the silver carbene complex (Figure 1a, b) [35,39]. Additionally, the carbene complex in ^{1}H NMR spectrum revealed a single set of signals with upfield shifts observed in the aromatic region relative to H_2-**L**$(PF_6)_2$. The characteristic olefin proton was found at δ = 7.33 ppm for $[Ag_2\mathbf{L}_2](PF_6)_2$ (Figure 1b). The ESI-MS spectrum further illustrated the generation of the binuclear tetracarbene complex (Figure S9).

The photochemical reaction of the silver carbene complex $[Ag_2\mathbf{L}_2](PF_6)_2$ was investigated by the irradiation of UV light (λ = 365 nm) (Figures S10–S16). In a typical experiment, the formation of photoproducts could be reliable and monitored by ^{1}H NMR spectra. As shown in Figure 1c, the olefinic signal totally disappeared and a new characteristic peak for the cyclobutane proton of $[Ag_2(\mathbf{L}')](PF_6)_2$ appeared at δ = 4.73 ppm [40–42]. The time-dependent ^{1}H NMR spectra indicated the photoreaction was completed in 15 min (Figure S15). The photoreaction conversion was also monitored by UV-vis and fluorescence experiments (Figure S16).

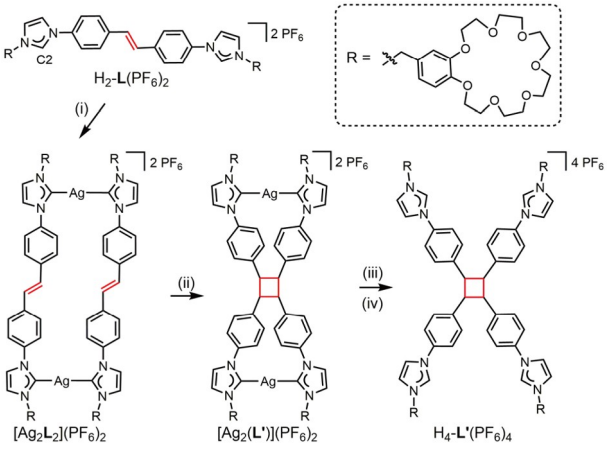

Scheme 2 Synthesis of silver carbene complex $[Ag_2\mathbf{L}_2](PF_6)_2$, photoproduct $[Ag_2(\mathbf{L}')](PF_6)_2$, and tetrakisimidazolium salt H_4-**L**′$(PF_6)_4$. (i) Ag_2O, CH_3CN, 65 °C, 24 h; (ii) *hv*, 365 nm; (iii) NH_4Cl, CH_3OH, rt, 4 h; (iv) NH_4PF_6, H_2O, rt, 6 h (color online).

Subsequently, the crown ether-based tetrakisimidazolium salt H_4-**L**′$(PF_6)_4$ was isolated by removing silver cations by treatment with an excess of NH_4Cl and subsequential anion exchange with NH_4PF_6. NMR and ESI-MS experiments confirmed the formation of expected composition of the demetallation product (Figures S17–S21). For example, the ^{1}H NMR spectrum of H_4-**L**′$(PF_6)_4$ in DMSO-d_6 displayed a set of characteristic peaks at δ = 9.81 and 4.80 ppm in a 1:1 ratio, indicating the complete demetallation of complex $[Ag_2(\mathbf{L}')](PF_6)_2$ (Figure 1d). The ESI-MS data provided further evidence for the isolation of tetrakisimidazolium salt, featuring the highest intensity for H_4-**L**′$(PF_6)_4$ at m/z = 749.0150 (calcd. for $[H_4\text{-}\mathbf{L}'(PF_6)]^{3+}$ 749.0020) (Figure S21).

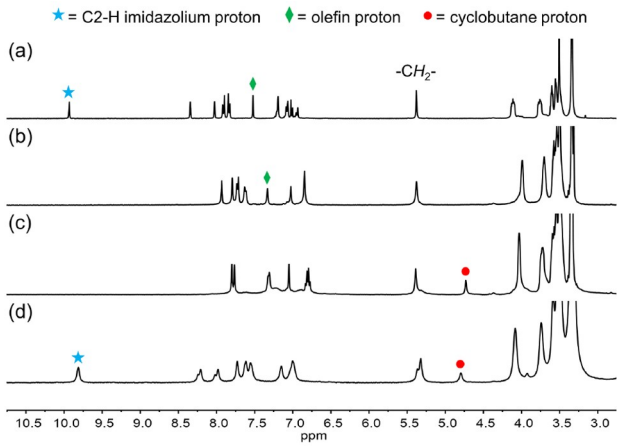

Figure 1 Partial ^{1}H NMR spectra (400 MHz, 298 K) in DMSO-d_6 of (a) bisimidazolium salt H_2-**L**$(PF_6)_2$, (b) before and (c) after UV irradiation of carbene complex $[Ag_2\mathbf{L}_2](PF_6)_2$, and (d) tetrakisimidazolium salt H_4-**L′**$(PF_6)_4$ (color online).

2.2 Preparation and characterization of SPN1

Further investigation of host-guest interaction in this multifunctional system *via* crown ether/bisammonium salt was carried out. As shown in Figure 2, the cyclobutane-based tetrakisimidazolium salt with crown ether units can serve as a building block to form a new polyimidazolium-based **SPN1**. It was found that the ^{1}H NMR spectrum of **SPN1** was convoluted, with each proton of B21C7 groups and ammonium units split into two sets of signals (Figure S22). It indicated the existence of cross-linked SPN and the slow-exchange nature of host-guest complexation on the NMR time scale [32]. Then, the concentration-dependent ^{1}H NMR spectra of the two-component system from 2.5 to 100 mM (based on the B21C7/ammonium salt units) were detected. With the concentration increases, the proton signals in ^{1}H NMR spectra became wider, which demonstrated the formation of **SPN1** was favored at high concentrations (Figure S23).

To further confirm the formation of **SPN1**, diffusion-ordered NMR spectroscopy (DOSY) was performed to investigate the size of the cross-linked SPN at 298 K (Figure 3a and Figures S24–S27). As the concentration of B21C7/ammonium salt units increased from 10 to 100 mM, the measured weight average diffusion coefficient (D) decreased from 3.16×10^{-9} to 5.01×10^{-10} m^2 s^{-1}, indicating the formation of supramolecular oligomers. Meanwhile, scanning electron microscopy (SEM) was employed to examine the morphology of **SPN1**, which was prepared by a freeze-drying method. The SEM result showed an extended and interconnected three-dimensional porous network (Figure 3b).

Then, the gelation process of **SPN1** was studied. The solution of functional imidazolium salt H_4-**L′**$(PF_6)_4$ and bisammonium salt **G** in CH_3CN was prepared in two vials (Figure S28, left). After adding bisammonium salt **G** solution into the solution of H_4-**L′**$(PF_6)_4$, supramolecular gel

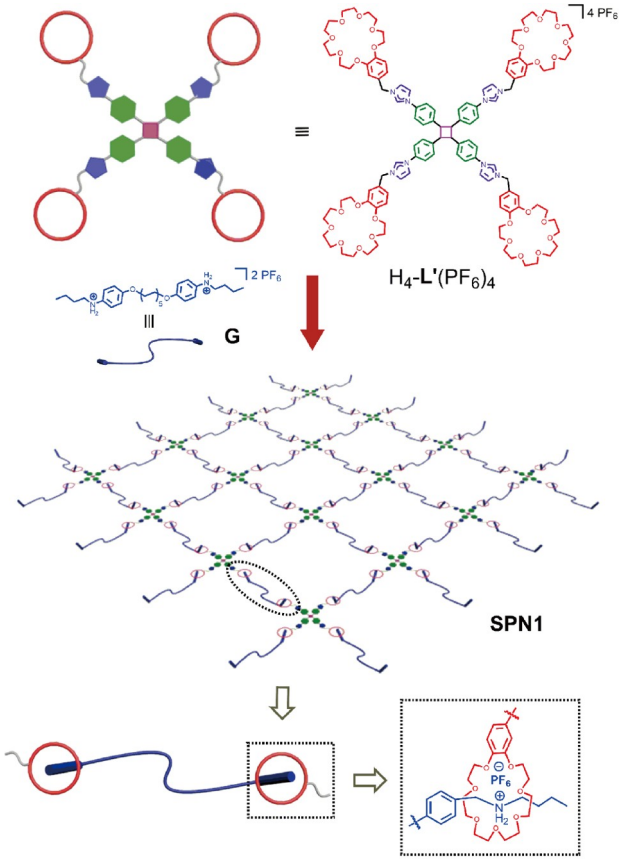

Figure 2 Formation of cross-linked **SPN1** from imidazolium salt H_4-**L′**$(PF_6)_4$ and bisammonium salt **G** (color online).

SPN1 was formed immediately (Figure S28, middle). In addition, the thermal reversibility of **SPN1** by an inverted vial experiment was investigated. Upon heating, the gel easily flowed at a high temperature as the decreased host-guest association constant. As the temperature returned to ambient levels, the gel recovered (Figure S28, middle and right).

To gain further insight into the supramolecular gel, the rheological characterization was performed at 298 K. **SPN1** was subjected to a strain scanning test to get broken strains with a sweep from 0.1% to 1,000%. As strain amplitude increased, the data displayed a broad gel region with a gel-to-sol cross-over point appearing at 216% strain (Figure 3c). The frequency sweep rheological experiment was performed from large (100 rad/s) to small (0.1 rad/s) angular frequency (ω). During this proceeding, the storage modulus (G') was always above the loss modulus (G'') (Figure 3d). These observations provided further evidence for the formation of the gel [43].

2.3 Antibacterial properties of SPN1

The antibacterial activity of **SPN1** was evaluated by plate counting method and Live/Dead Baclight assay. As shown in Figure 4, **SPN1** showed a dose-dependent antibacterial

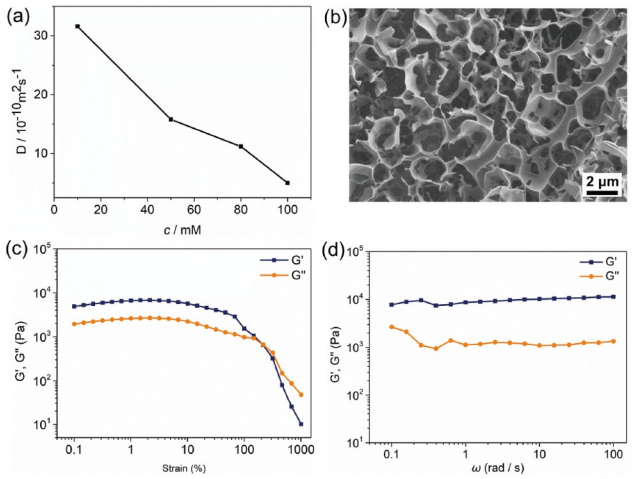

Figure 3 (a) Concentration dependence of D (600 MHz, CD_3CN, 298 K) of **SPN1** at different crown ether unit concentrations: 10, 50, 80 and 100 mM (based on the B21C7/ammonium salt units). (b) SEM image of **SPN1** prepared by a freeze-drying method (T = 298 K). (c, d) Rheological characterization (T = 298 K) of **SPN1**. Here are the storage modulus (G') and loss modulus (G'') *versus* strain (%) and frequency (ω) for the samples (color online).

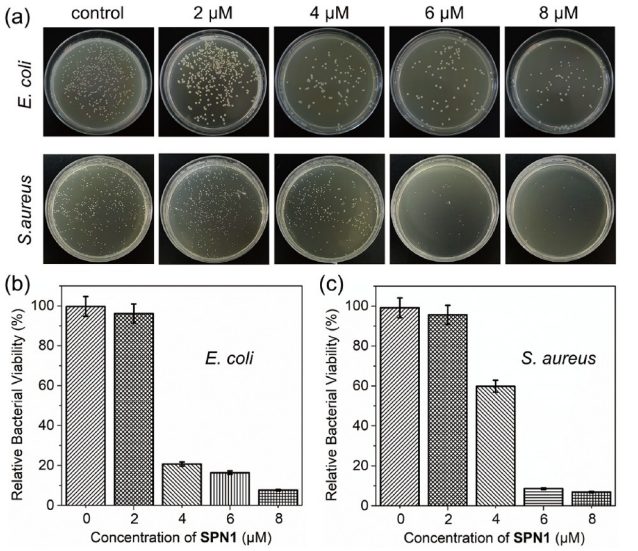

Figure 4 (a) Bacterial colony formation of *E. coli* and *S. aureus*. Relative bacterial viability of (b) *E. coli* and (c) *S. aureus* under different concentrations of **SPN1** (color online).

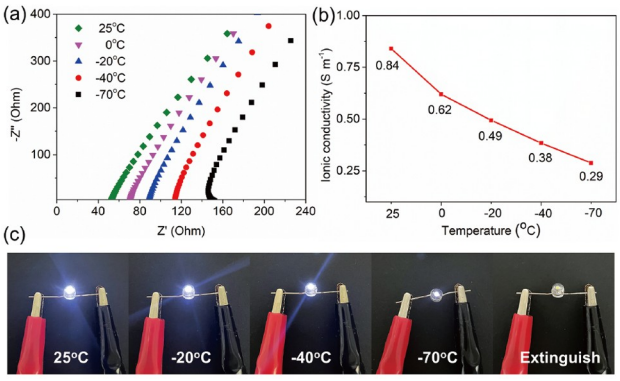

Figure 5 (a) Nyquist plots and (b) conductivities of **SPN1** at 25, 0, −20, −40 and −70 °C. (c) Comparison of luminance of LEDs (working voltage of 9 V) by using **SPN1** as a conductor at varying temperatures (color online).

ability against both *E. coli* and *S. aureus* as representative Gram-negative and Gram-positive bacteria, respectively. Treatment with 8 μM of **SPN1** resulted in a significant reduction in bacterial viability, with 7.6% for *E. coli* and 6.9% for *S. aureus*, revealing that **SPN1** could effectively inhibit the bacterial growth in both strains. Noting that **SPN1** showed better antibacterial ability than that of tetrakisimidazolium salt H_4-**L′**$(PF_6)_4$ against *E. coli* and *S. Aureus* (Figure S29). In contrast, the bisimidazolium salt H_2-**L**$(PF_6)_2$ had almost no antibacterial activity (Figure S30).

The antibacterial capacity was also conducted by confocal laser scanning microscopy (CLSM). As the CLSM images in Figure S31, few red fluorescence spots could be seen in the control group, but the more visible red spots appeared in both *E. coli* and *S. aureus* on treatment with **SPN1**, which further verified the good antibacterial capability of **SPN1**.

2.4 Conductivity and anti-freezing properties of SPN1

Imidazolium salts are well-known as a type of ionic liquid due to their noteworthy characteristics, such as relatively high intrinsic conductivity, thermal and chemical stability and environmental friendliness [44,45]. Then, the electrical behavior of **SPN1** was investigated. As shown in Figure S32, **SPN1** was used as a conductor to connect light-emitting diode (LED) and battery, and the LED lighted when the power source was turned on. The conductivity of **SPN1** was also characterized by electrochemical impedance spectroscopy (EIS), which showed the conductivity value was 0.84 S m^{-1} at 25 °C (Figure 5a, b). The conductivity of the gel is comparable or superior to the most reported ionic liquids [46,47]. Compared with **SPN1**, the conductivity of tetrakisimidazolium salt H_4-**L′**$(PF_6)_4$ is negligible (~10^{-5} S m^{-1}) (Figure S33). It means that a significant improvement in conductivity arises from the formation of SPN.

With the expanded application of the gel in extreme conditions, especially cryogenic conditions, the temperature dependence of EIS and conductivity tests for **SPN1** in the temperature range from 25 to −70 °C were also investigated. The result demonstrated that the conductivity reduced from 0.84 to 0.29 S m^{-1} with the temperature decrease (Figure 5a, b). The decreased conductivity at low temperatures could be related to the slower and restricted ion mobility of the gel [48,49]. In addition, the conductivity performance of **SPN1** was further demonstrated by serving as a conductor in a circuit to light LED at different temperatures (Figure 5c). With the decrease in temperature, the luminance of LED

became weaker. Surprisingly, the LED could be lightened even at −70 °C, indicating that the gel has excellent anti-freezing properties.

3 Conclusions

In summary, we have developed a supramolecular controlled topochemical reaction strategy to construct functionalized polyimidazolium derivative H_4-**L′**$(PF_6)_4$ with crown ether groups at each *N*-wingtip, which cannot be obtained by a single-step synthesis route in organic chemistry. The polyimidazolium salt H_4-**L′**$(PF_6)_4$ with B21C7 units could be extended into a cross-linked supramolecular polymer network with multiple functions upon the addition of secondary ammonium guests. Compared with tetrakisimidazolium salt H_4-**L′**$(PF_6)_4$, the antibacterial activity and conductivity of **SPN1** were greatly improved. By employing this strategy, the construction of SPN with devisable functions has become feasible and practicable. Further investigation into using the supramolecular gel as a portable material is ongoing.

Acknowledgements This work was supported by the National Natural Science Fund for Distinguished Young Scholars of China (22025107), Shaanxi Fundamental Science Research Project for Chemistry & Biology (22JHZ003), the National Youth Top-notch Talent Support Program of China, Xi'an Key Laboratory of Functional Supramolecular Structure and Materials, and the FM&EM International Joint Laboratory of Northwest University.

Conflict of interest The authors declare no conflict of interest.

Supporting information The supporting information is available online at http://chem.scichina.com and http://link.springer.com/journal/11426. The supporting materials are published as submitted, without typesetting or editing. The responsibility for scientific accuracy and content remains entirely with the authors.

1 Yang L, Tan X, Wang Z, Zhang X. *Chem Rev*, 2015, 115: 7196–7239
2 Voorhaar L, Hoogenboom R. *Chem Soc Rev*, 2016, 45: 4013–4031
3 Han W, Xiang W, Li Q, Zhang H, Yang Y, Shi J, Ji Y, Wang S, Ji X, Khashab NM, Sessler JL. *Chem Soc Rev*, 2021, 50: 10025–10043
4 Yan X, Wang F, Zheng B, Huang F. *Chem Soc Rev*, 2012, 41: 6042–6065
5 Lu W, Le X, Zhang J, Huang Y, Chen T. *Chem Soc Rev*, 2017, 46: 1284–1294
6 Yanagisawa Y, Nan Y, Okuro K, Aida T. *Science*, 2018, 359: 72–76
7 Wang S, Urban MW. *Nat Rev Mater*, 2020, 5: 562–583
8 Tee BCK, Wang C, Allen R, Bao Z. *Nat Nanotech*, 2012, 7: 825–832
9 Webber MJ, Appel EA, Meijer EW, Langer R. *Nat Mater*, 2016, 15: 13–26
10 Liu K, Jiang Y, Bao Z, Yan X. *CCS Chem*, 2019, 1: 431–447
11 Huang X, Li R, Duan Z, Xu F, Li H. *Soft Matter*, 2022, 18: 3828–3844
12 Xia D, Wang P, Ji X, Khashab NM, Sessler JL, Huang F. *Chem Rev*, 2020, 120: 6070–6123
13 Guo C, Su F, Su P, Yu X, Li X. *Sci China Chem*, 2023, 66: 1940–1962
14 Zhang M, Yin S, Zhang J, Zhou Z, Saha ML, Lu C, Stang PJ. *Proc Natl Acad Sci USA*, 2017, 114: 3044–3049
15 Tao R, Zhang Q, Rao S, Zheng X, Li M, Qu D. *Sci China Chem*, 2019, 62: 245–250
16 Gao K, Feng Q, Zhang Z, Zhang R, Hou Y, Mu C, Li X, Zhang M. *Angew Chem Int Ed*, 2022, 61: e202209958
17 Xue Y, Jiang S, Zhong H, Chen Z, Wang F. *Angew Chem Int Ed*, 2022, 61: e202110766
18 Zhang ZE, Zhang YF, Zhang YZ, Li HL, Sun LY, Wang LJ, Han YF. *J Am Chem Soc*, 2023, 145: 7446–7453
19 Wang XQ, Wang W, Yin GQ, Wang YX, Zhang CW, Shi JM, Yu Y, Yang HB. *Chem Commun*, 2015, 51: 16813–16816
20 Ji X, Ahmed M, Long L, Khashab NM, Huang F, Sessler JL. *Chem Soc Rev*, 2019, 48: 2682–2697
21 Huang Z, Chen X, O'Neill SJK, Wu G, Whitaker DJ, Li J, McCune JA, Scherman OA. *Nat Mater*, 2022, 21: 103–109
22 Avestro AJ, Belowich ME, Stoddart JF. *Chem Soc Rev*, 2012, 41: 5881–5895
23 Liu Z, Nalluri SKM, Stoddart JF. *Chem Soc Rev*, 2017, 46: 2459–2478
24 Fang W, Zhang Y, Wu J, Liu C, Zhu H, Tu T. *Chem – An Asian J*, 2018, 13: 712–729
25 Kumar R, Sharma A, Singh H, Suating P, Kim HS, Sunwoo K, Shim I, Gibb BC, Kim JS. *Chem Rev*, 2019, 119: 9657–9721
26 Hu Y, Long S, Fu H, She Y, Xu Z, Yoon J. *Chem Soc Rev*, 2021, 50: 589–618
27 Wang Y, Chang JP, Xu R, Bai S, Wang D, Yang GP, Sun LY, Li P, Han YF. *Chem Soc Rev*, 2021, 50: 13559–13586
28 Wang W, Zhang Y, Sun B, Chen LJ, Xu XD, Wang M, Li X, Yu Y, Jiang W, Yang HB. *Chem Sci*, 2014, 5: 4554–4560
29 Lu C, Zhang M, Tang D, Yan X, Zhang ZY, Zhou Z, Song B, Wang H, Li X, Yin S, Sepehrpour H, Stang PJ. *J Am Chem Soc*, 2018, 140: 7674–7680
30 Zhang Q, Tang D, Zhang J, Ni R, Xu L, He T, Lin X, Li X, Qiu H, Yin S, Stang PJ. *J Am Chem Soc*, 2019, 141: 17909–17917
31 Wu Y, Shangguan L, Li Q, Cao J, Liu Y, Wang Z, Zhu H, Wang F, Huang F. *Angew Chem Int Ed*, 2021, 60: 19997–20002
32 Zhang ZE, An YY, Zheng B, Chang JP, Han YF. *Sci China Chem*, 2021, 64: 1177–1183
33 Shentu Z, Zhang Z, Zhao J, Chen C, Wu Q, Wang L, Yan X. *J Mater Chem A*, 2021, 9: 19619–19624
34 Zhao Y, Song S, Ren X, Zhang J, Lin Q, Zhao Y. *Chem Rev*, 2022, 122: 5604–5640
35 Gan MM, Liu JQ, Zhang L, Wang YY, Hahn FE, Han YF. *Chem Rev*, 2018, 118: 9587–9641
36 Sun LY, Sinha N, Yan T, Wang YS, Tan TTY, Yu L, Han YF, Hahn FE. *Angew Chem Int Ed*, 2018, 57: 5161–5165
37 Gou XX, Liu T, Wang YY, Han Y-. *Angew Chem Int Ed*, 2020, 59: 16683–16689
38 Han YF, Jin GX, Hahn FE. *J Am Chem Soc*, 2013, 135: 9263–9266
39 Ibáñez S, Poyatos M, Peris E. *Acc Chem Res*, 2020, 53: 1401−1413
40 Biradha K, Santra R. *Chem Soc Rev*, 2013, 42: 950–967
41 Li Y, Jin GF, An YY, Das R, Han YF. *Chin J Chem*, 2019, 37: 1147–1152
42 Guadalupe Vasquez-Ríos M, Campillo-Alvarado G, MacGillivray LR. *Angew Chem Int Ed*, 2023, 62: e202308350
43 Zhao X, Chen F, Li Y, Lu H, Zhang N, Ma M. *Nat Commun*, 2018, 9: 3579
44 Goossens K, Lava K, Bielawski CW, Binnemans K. *Chem Rev*, 2016, 116: 4643–4807
45 Correia DM, Fernandes LC, Martins PM, García-Astrain C, Costa CM, Reguera J, Lanceros-Méndez S. *Adv Funct Mater*, 2020, 30: 1909736
46 Pandey GP, Hashmi SA. *J Mater Chem A*, 2013, 1: 3372–3378
47 Serra JP, Fernandes LC, Correia DM, Tubio CR, Vilas-Vilela JL, Tariq M, Esperança JMSS, Costa CM, Lanceros-Mendez S. *Mater Adv*, 2022, 3: 937–945
48 Ye Y, Zhang Y, Chen Y, Han X, Jiang F. *Adv Funct Mater*, 2020, 30: 2003430
49 Luo Z, Li W, Yan J, Sun J. *Adv Funct Mater*, 2022, 32: 2203988